Supplementary figures and figure legends

Supplementary figure 1

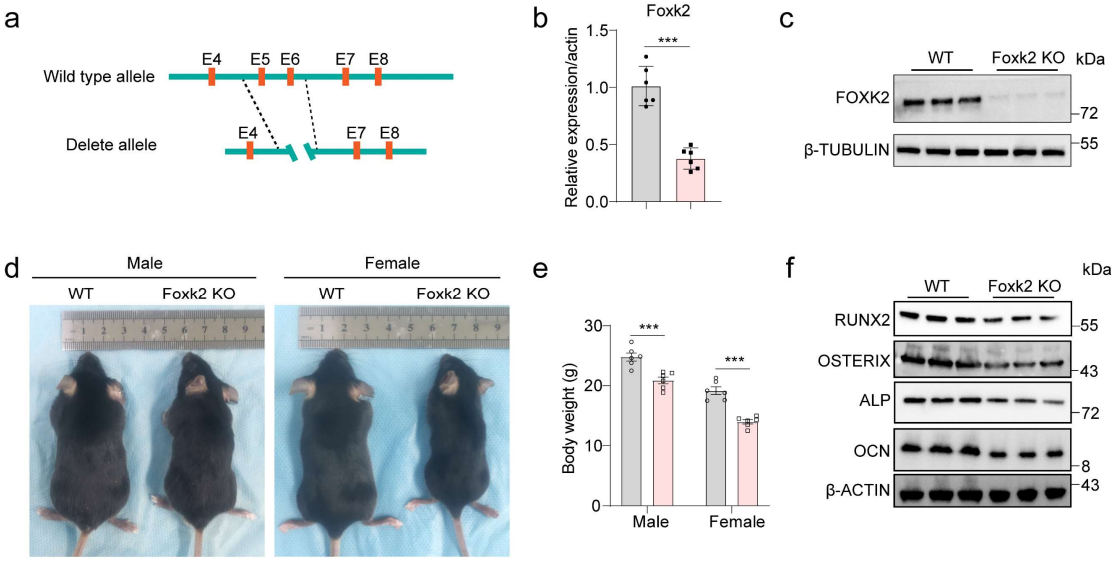

Supplementary figure 1. Construction and identification of *Foxk2 KO* mice. (a) Schematic diagram of wild-type and mutant alleles. (b) qPCR quantified mRNA levels of Foxk2 in the femurs of WT and *Foxk2 KO* mice ($n=6$). (c) Western blot analysis of Foxk2 protein in the femurs of WT and *Foxk2 KO* mice. (d) Representative images of the male and female WT and *Foxk2 KO* mice at 8 weeks old. (e) Body weight of male and female WT and *Foxk2 KO* mice at 8 weeks old ($n=6$). (f) Western blot analysis of RUNX2, OSTERIX, ALP and OCN in the femurs of WT and *Foxk2 KO* mice. ***$p < 0.001$.

Supplementary figure 2

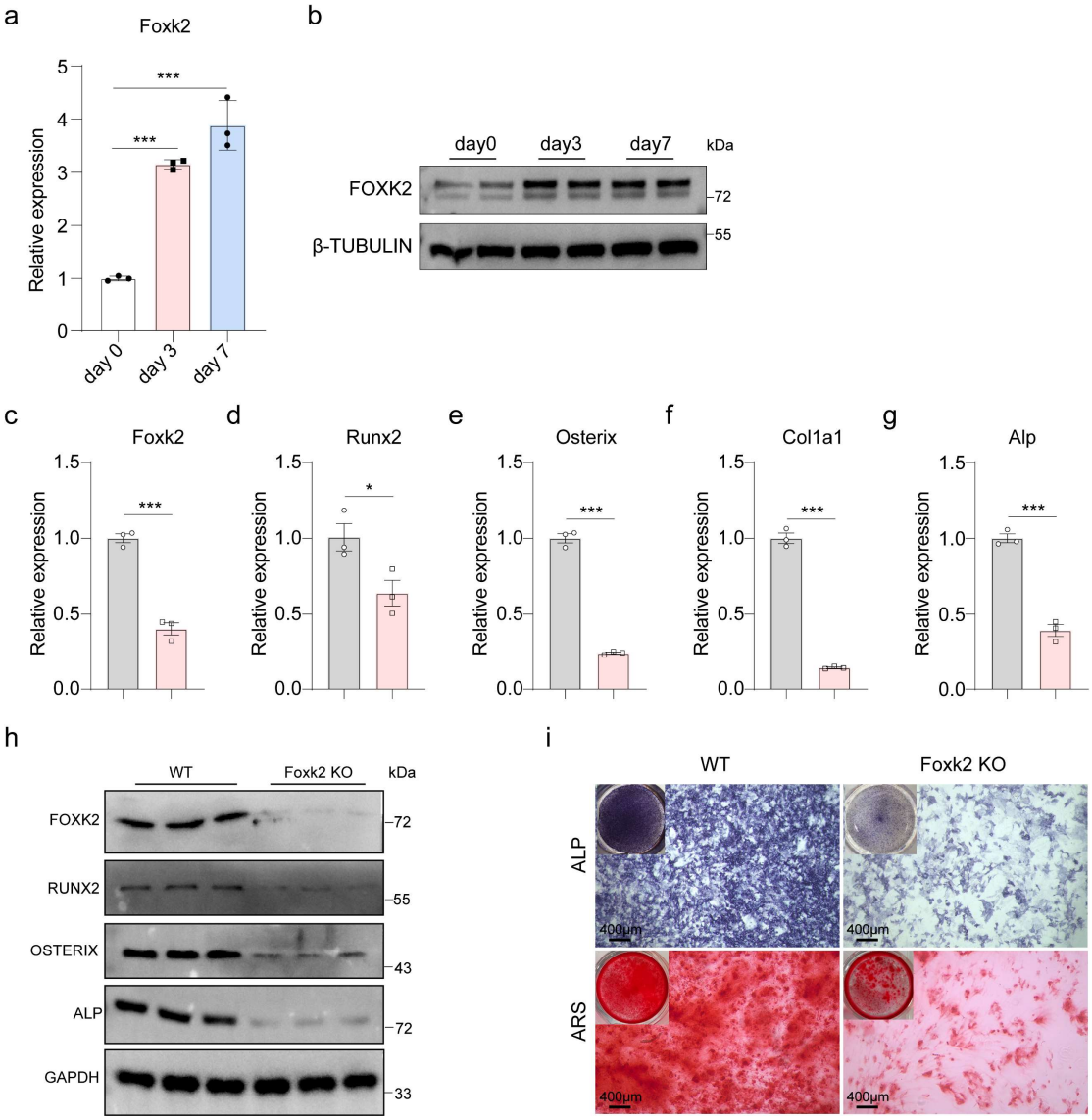

Supplementary figure 2. Foxk2 plays a positive role in osteoblast differentiation. (a) qPCR quantified mRNA levels of Foxk2 in osteoblasts induced osteogenic differentiation on day 0, 3, and 7 (*n=3*). (b) Western blot detection of FOXK2 protein in osteoblasts induced osteogenic differentiation on day 0, 3, and 7. (c-g) qPCR quantified mRNA levels of Foxk2 (c), Runx2 (d), Osterix (e), Col1a1 (f) and Alp (g) in WT and *Foxk2 KO* primary pre-osteoblasts (*n=3*). (h) Western blot analysis of FOXK2, RUNX2, OSTERIX and ALP in WT and *Foxk2 KO* primary pre-osteoblasts. (i) Representative images of ALP and ARS staining of *WT* and *Foxk2 KO* primary pre-osteoblasts. *$p < 0.05$, ***$p < 0.001$.

Supplementary figure 3

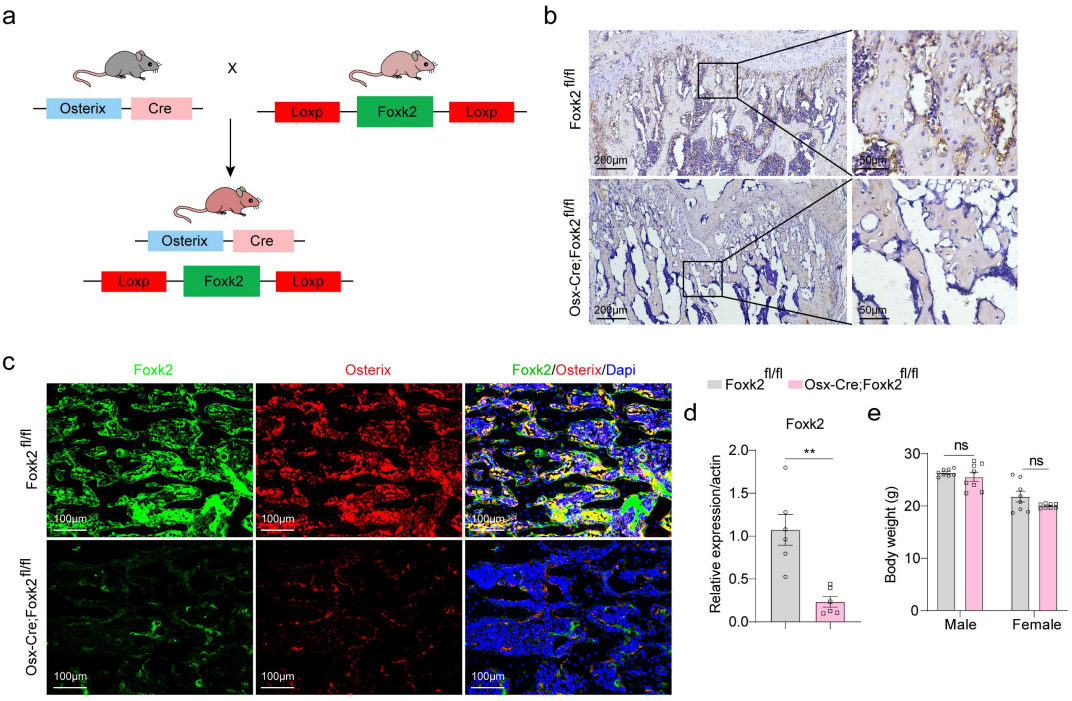

Supplementary figure 3. Construction and identification of *Osx-Cre;Foxk2$^{fl/fl}$* mice. (a) Schematic diagram of Generation of *Osx-cre;Foxk2$^{fl/fl}$* mice. (b) Representative images of FOXK2 IHC staining of the femurs in *Foxk2$^{fl/fl}$* and *Osx-Cre;Foxk2$^{fl/fl}$* mice. (c) Representative images of FOXK2 and OSTERIX IF staining of the femurs in *Foxk2$^{fl/fl}$* and *Osx-Cre;Foxk2$^{fl/fl}$* mice. (d) qPCR quantified mRNA levels of Foxk2 in the femurs *Foxk2$^{fl/fl}$* and *Osx-Cre;Foxk2$^{fl/fl}$* mice($n=6$). (d) Body weight of male and female *Foxk2$^{fl/fl}$* and *Osx-Cre;Foxk2$^{fl/fl}$* mice at 8 weeks old ($n=8$). $^{**}p < 0.01$.

Supplementary figure 4

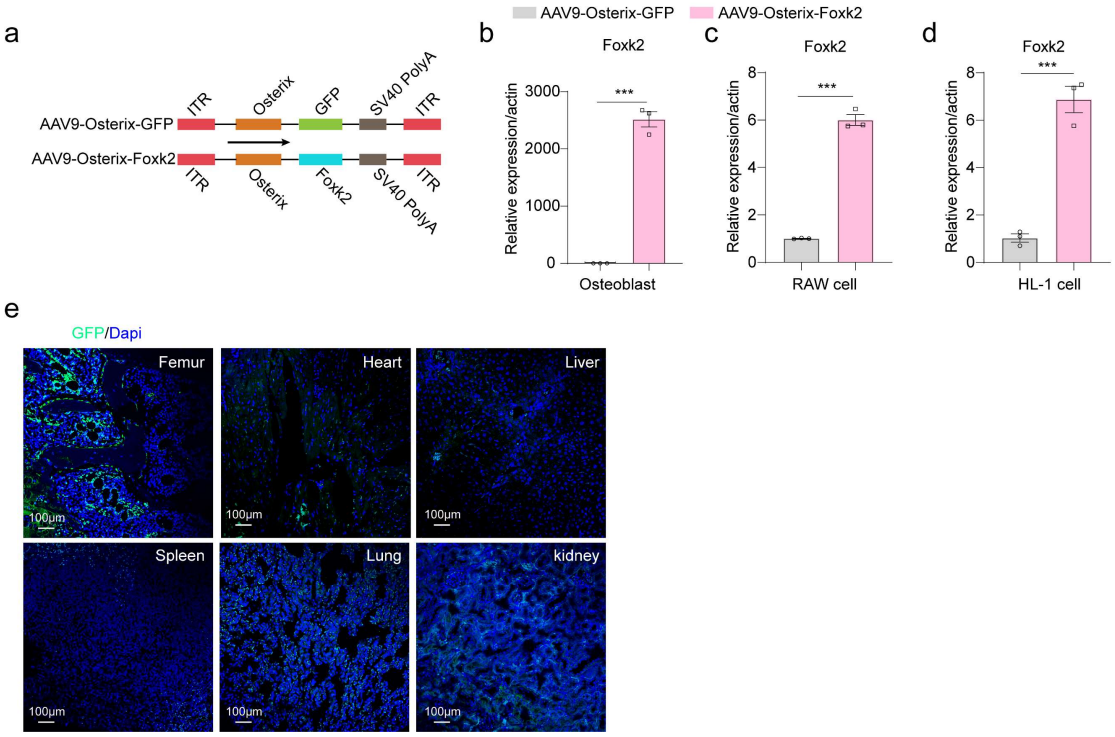

Supplementary figure 4. Identification of the targeting of pre-osteoblast specific promoter (Osterix) modified AAV9 vector *in vitro* and *in vivo*. (a) Schematic diagram of AAV9 vector. (b-d) qPCR analysis of mRNA levels of Foxk2 in primary osteoblasts (b), RAW cells (c), and HL-1 cells (d) treated with AAV9-Osterix-GFP or AAV9-Osterix-Foxk2 for 3 days of ($n=3$). (e) Representative IF staining images of GFP in femur, heart, liver, spleen, lung and kidney from treated with AAV9-Osterix-GFP mice. $^{**}p < 0.01$.

Supplementary figure 5

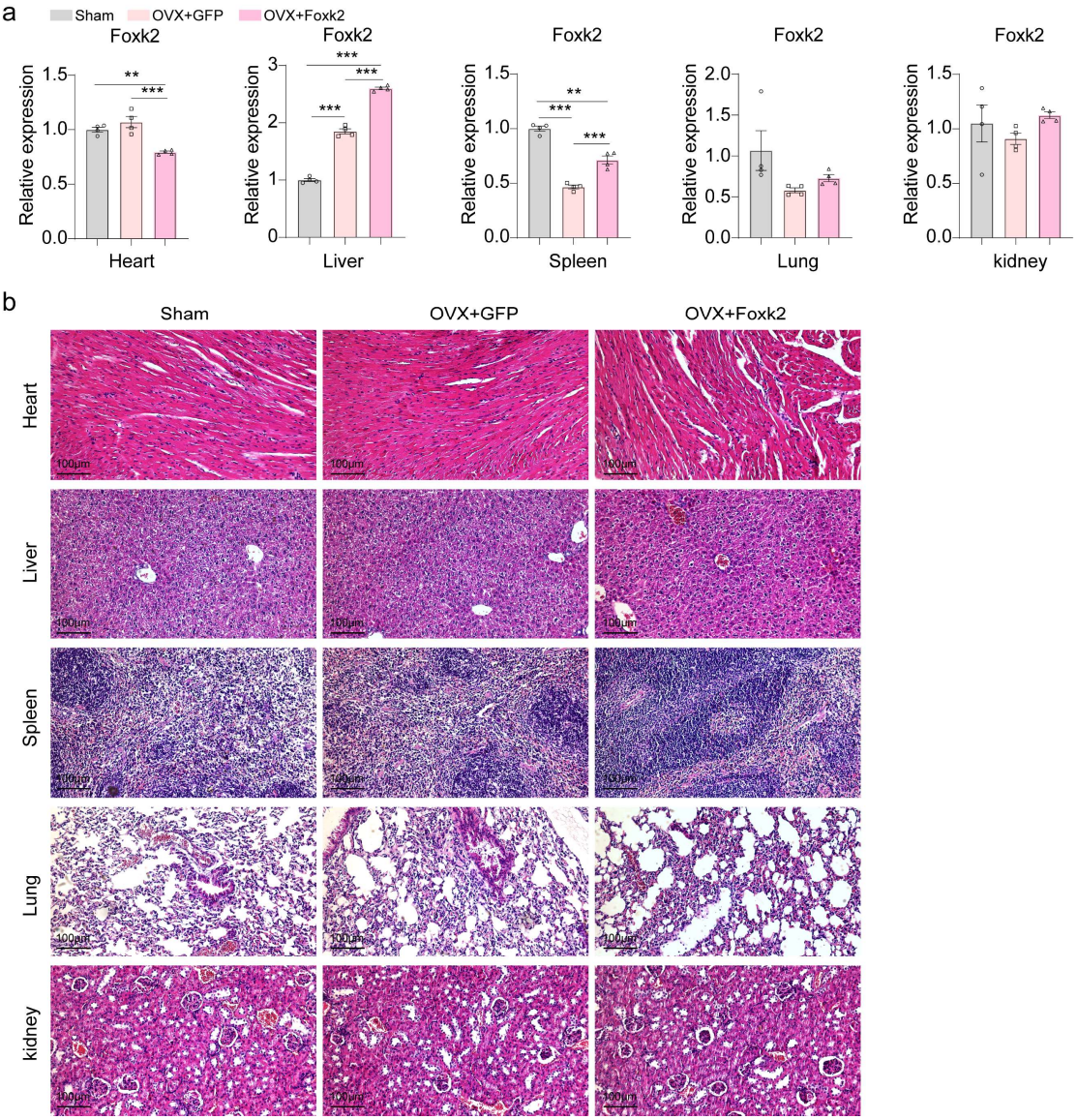

Supplementary figure 5. Pre-osteoblast specific promoter (Osterix) modified AAV9 vector possessed favorable bone targeting *in vivo*. (a) qPCR analysis of mRNA levels of Foxk2 in heart, liver, spleen, lung and kidney from treated sham and OVX mice (*n=4*). (b) Representative H&E staining images of heart, liver, spleen, lung and kidney in treated sham and OVX mice. ***p < 0.01, ****p < 0.001*.

Supplementary figure 6

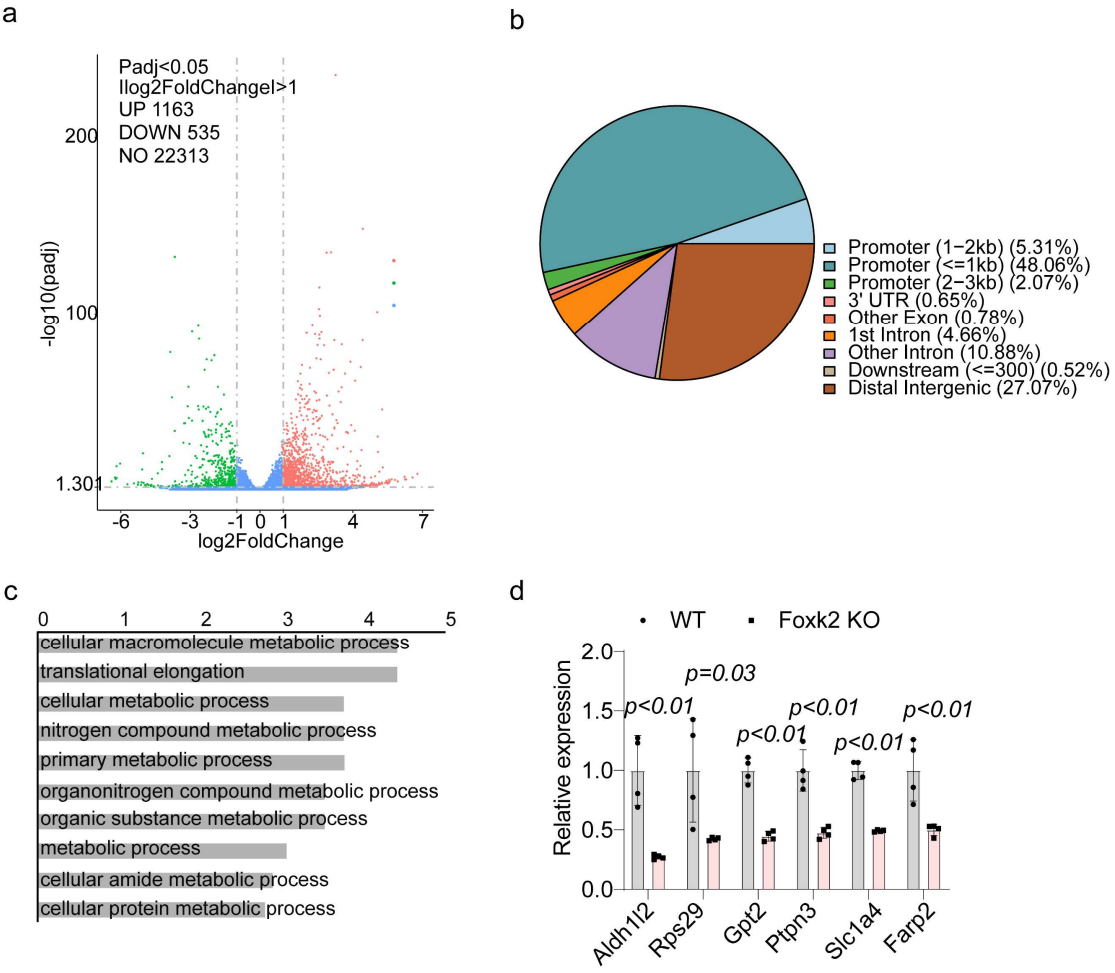

Supplementary figure 6. RNA-seq and CUT&Tag were used to detect downstream of Foxk2 in regulating osteoblast differentiation. (a) Volcano plot: The upregulated genes (1163) are represented by red dots, and the downregulated genes (535) are represented by green dots. The blue dots indicate non-significant differentially expressed genes. (b) FOXK2-binding motif identified by MEME-ChIP *de novo* motif search. (c) Gene Ontology (GO) analysis of genes is bound by FOXK2 in CUT&Tag data. (d) qPCR further validated the expression of candidate genes in *Foxk2 KO* pre-osteoblasts.

Supplementary figure 7

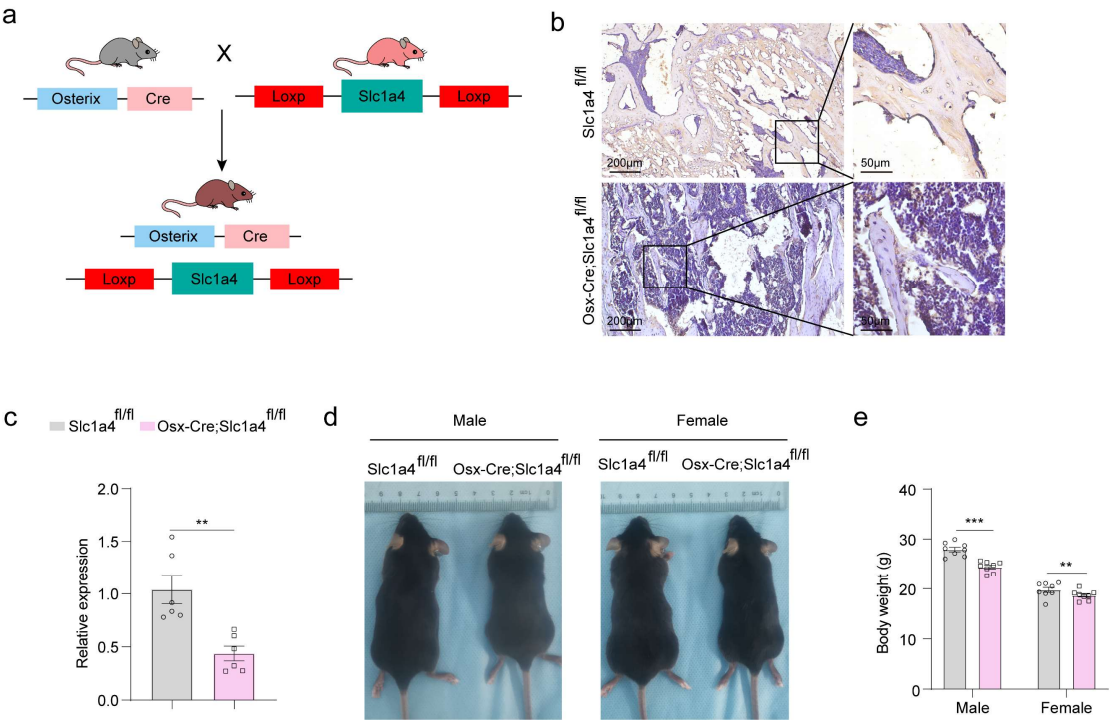

Supplementary figure 7. Construction and identification of *Osx-Cre;Slc1a4$^{fl/fl}$* mice. (a) Schematic diagram of Generation of *Osx-cre;Slc1a4$^{fl/fl}$* mice. (b) Representative images of SLC1A4 IHC staining of the femurs in *Slc1a4$^{fl/fl}$* and *Osx-Cre;Slc1a4$^{fl/fl}$* mice. (c) qPCR quantified mRNA levels of Slc1a4 in the femurs of *Slc1a4$^{fl/fl}$* and *Osx-Cre;Slc1a4$^{fl/fl}$* mice (*n=6*). (d) Representative images of the male and female *Slc1a4$^{fl/fl}$* and *Osx-Cre;Slc1a4$^{fl/f}$* mice at 8 weeks old. (e) Body weight of male and female *Slc1a4$^{fl/fl}$* and *Osx-Cre;Slc1a4$^{fl/f}$* mice at 8 weeks old (*n=8*). $^{**}p < 0.01$.

Supplementary figure 8

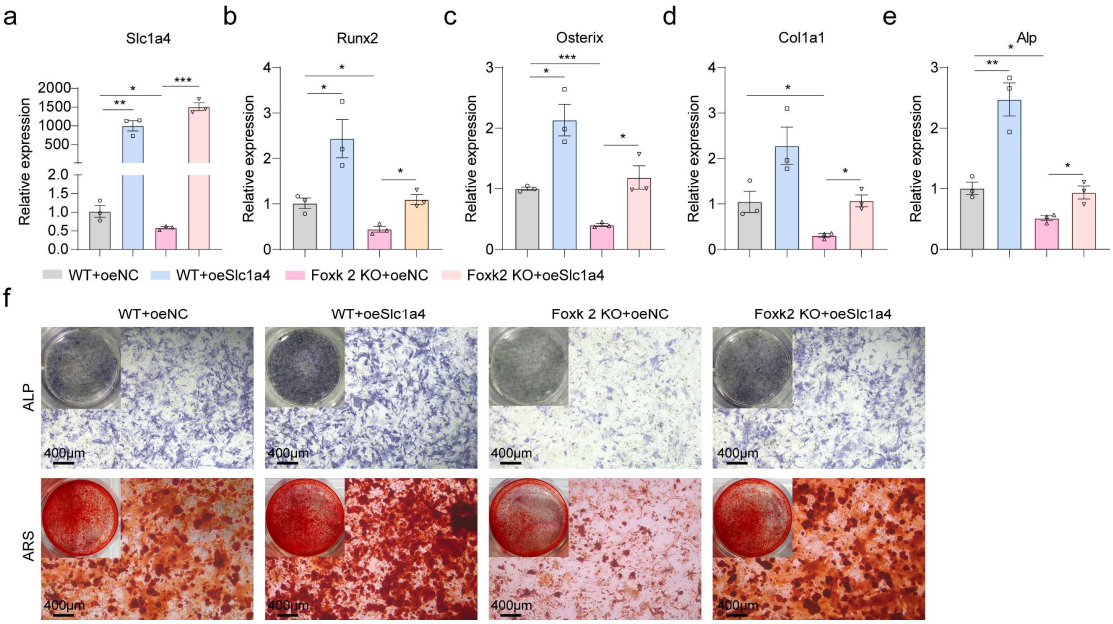

Supplementary figure 8. Slc1a4 functions as a direct downstream mediator of Foxk2 in osteoblast differentiation. (a-e) mRNA levels of Slc1a4 (a), Runx2 (b), Osterix (c), Col1a1 (d) and Alp (e) in WT and *Foxk2 KO* primary pre-osteoblasts treated with control plasmids or Slc1a4 overexpression plasmids (*n=3*). (f) Representative images of ALP and ARS staining of WT and *Foxk2 KO* primary pre-osteoblasts treated with control plasmids or Slc1a4 overexpression plasmids. $**p < 0.05$, $**p < 0.01$, $***p < 0.001$.

Supplementary figure 9

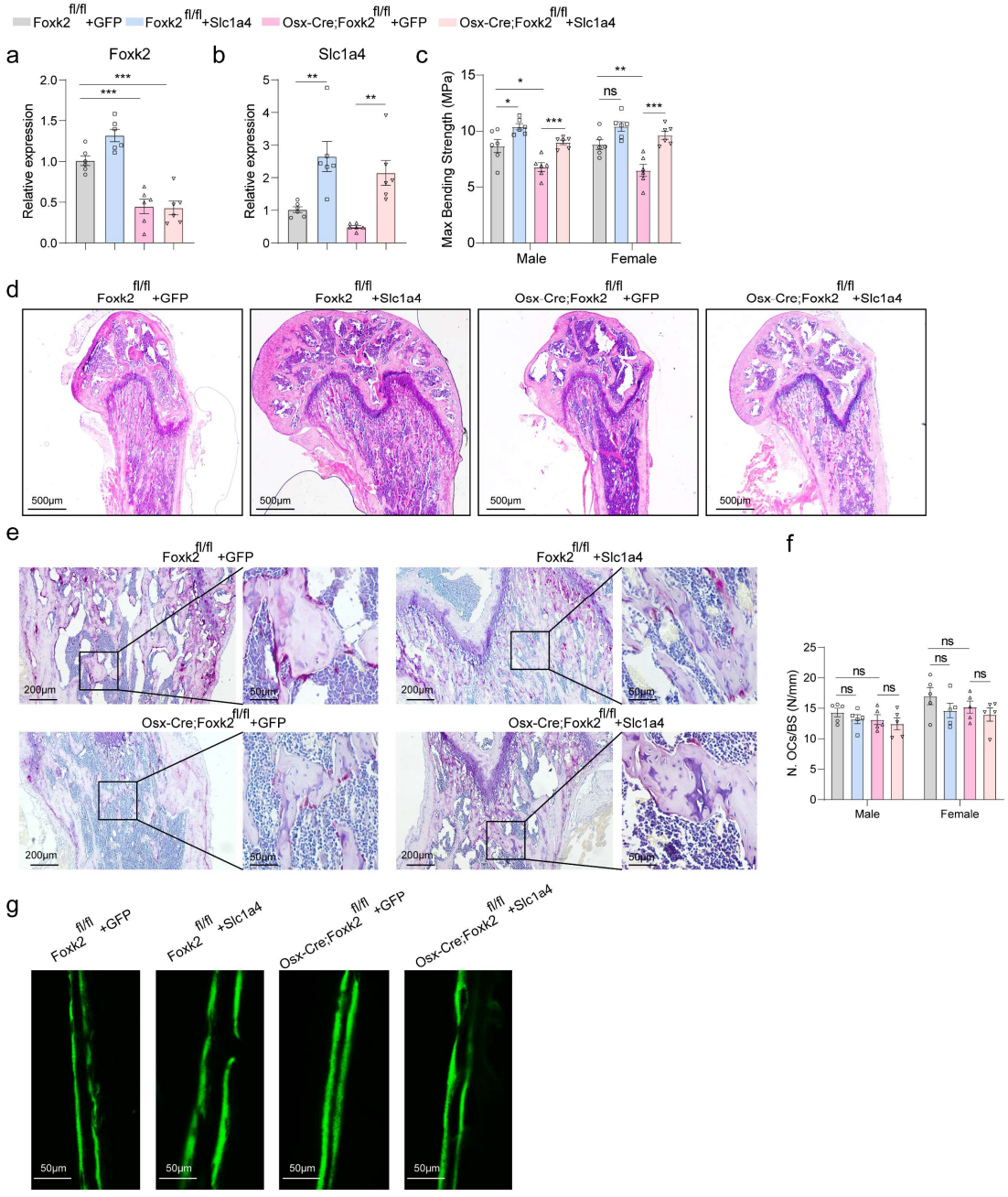

Supplementary figure 9. Slc1a4 functions as a direct downstream mediator of Foxk2 in bone formation. (a) mRNA levels of Foxk2 in the femurs of treated *Foxk2*$^{fl/fl}$ and *Osx-Cre;Foxk2*$^{fl/fl}$ mice ($n=6$). (b) mRNA levels of Slc1a4 in the femurs of treated *Foxk2*$^{fl/fl}$ and *Osx-Cre;Foxk2*$^{fl/fl}$ mice ($n=6$). (c) Quantitative analysis of biomechanics of the femurs from treated male and female *Foxk2*$^{fl/fl}$ and *Osx-Cre;Foxk2*$^{fl/fl}$ mice ($n=6$), characterized as Maximal Bending Strength. (d) Representative images of H&E staining of treated female *Foxk2*$^{fl/fl}$ and *Osx-*

Cre;Foxk2$^{fl/fl}$ mice. (e) Representative images of TRAP staining of treated male *Foxk2*$^{fl/fl}$ and *Osx-Cre;Foxk2*$^{fl/fl}$ mice. (f) Quantification of TRAP staining of treated male and female *Foxk2*$^{fl/fl}$ and *Osx-Cre;Foxk2*$^{fl/fl}$ mice ($n=5$). (g) Representative images of calcein double labeling of treated female *Foxk2*$^{fl/fl}$ and *Osx-Cre;Foxk2*$^{fl/fl}$ mice. $*p < 0.05$, $**p < 0.01$, $***p < 0.001$.

Supplementary figure 10

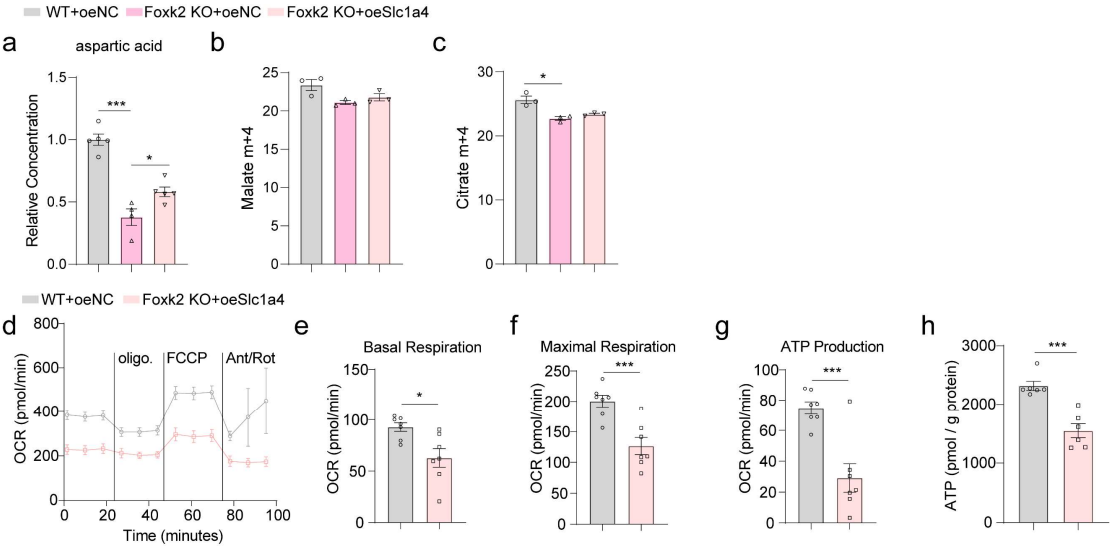

Supplementary figure 10. Deletion of Foxk2 suppress mitochondrial oxidative phosphorylation and ATP production. (a) Effect of Foxk2/Slc1a4 axis on intracellular aspartic acid concentration measured by mass spectrometry in WT and *Foxk2 KO* primary pre-osteoblasts treated with control plasmids or Slc1a4 overexpression plasmids (WT+oeNC: *n=5*, Foxk2 KO+oeNC: *n=4*, Foxk2 KO+oeSlc1a4: *n=6*). (b and c) Isotopic labeling of malate (b), and citrate (c) (*n=3*). (d-g) The oxygen consumption rate in WT and *Foxk2 KO* primary pre-osteoblasts was measured using Seahorse XF assay. Basal respiration (e), Maximal respiration (f) and ATP production (g) were analyzed (*n=7*). (h) Relative content of ATP in WT and *Foxk2 KO* primary pre-osteoblasts (*n=6*). *$p < 0.05$, ***$p < 0.001$.

104 **Table S1. Primers for genotyping.**

PRIMER TYPE	SEQUENCE 5' → 3'
Foxk2 KO-loxp-F	TAACTCCTGGGCTTTGCTGACTTGC
Foxk2 KO-loxp-R	CCTGGTGATGAGCTGAGTGAGACTG
Foxk2KO-Mut-F	TAACTCCTGGGCTTTGCTGACTTGC
Foxk2KO-Mut-R	GCTTGCTTTTGTGTCAGTGCACCAT
Foxk2-loxP-F	TGGCTTATGTCTGCTGTTTGTCTC
Foxk2-loxP-R	GTTTCTAAGGAACCAGTCAGCAGG
Osx-Cre-Common F	TACCAGAAGCGACCACTTGAGC
Osx-Cre-WT-R	CGCCAAGAGAGCCTGGCAAG
Osx-Cre-Mut-R	GCACACAGACAGGAGCATCTTC
Slc1a4-loxP-F	CCACATGGCTCCTGAAAATCTCAT
Slc1a4-loxP-R	GGCTGTTAGAACATTCCTTCAGAGA

105

106 **Table S2, siRNAs sequences.**

Gene	Sense (5'-3')	Antisense (3'-5')
Slc1a4	CCUUCAAUGAGGCCACAAUTT	AUUGUGGCCUCAUUGAAGGTT
Aldh1l2	CCUUGAGCUUGGUGGCAAATT	UUUGCCACCAAGCUCAAGGTT
Farp2	GGAGAUUCUCGCUACAGAATT	UUCUGUAGCGAGAAUCUCCTT
Ptpn3	GCUCGUGGUCUCGAGGAUATT	UAUCCUCGAGACCACGAGCTT
Rps29	GCUAGUCUUUGUACACAAATT	UUUGUGUACAAAGACUAGCTT
Gpt2	CCAUGGACAUUGUUGUGAATT	UUCACAACAAUGUCCAUGGTT

107

Table S3. qPCR primer sequence.

PRIMER TYPE	SEQUENCE 5' → 3'
mus Foxk2-F	CCACGGGAACTATCAGTGCT
mus Foxk2-R	GTCATCCTTTGGGCTGTCTC
mus Runx2-F	ATGAGAGTAGGTGTCCCGCC
mus Runx2-R	GTGGAGTGGATGGATGGGGA
mus Osterix-F	GGCAAGAGGTTCACTCGCTC
mus Osterix-R	CTTGGAACAGAGCAGGCAGG
mus Alp-F	CAACCTGACTGACCCTTCGC
mus Alp-R	CAGAGCCTGCTTGGCCTTAC
mus Ocn-F	CAAGTCCCACACAGCAGCTT
mus Ocn-R	AAAGCCGAGCTGCCAGAGTT
mus Col1a1-F	CTCAGGGTGCTCGTGGATTC
mus Col1a1-R	CTCACCAGGGGAACCACTCT
mus Slc1a4-F	CTACAAGAAGTGAAGGTGGAAGCC
mus Slc1a4-R	TGGATTCAAGTTCAGGAGCAATGG
mus Farp2-F	ATGGTCTGTTCCTCATTGCTTCAC
mus Farp2-R	ATAGTCTTGGCTGCTTGGATTGC
mus Ptpn3-F	TGCCGACAGCCAGTTCATACC
mus Ptpn3-R	GCTCCACTCCGTAGAAGTCAAGG
mus Rps29-F	AGTCACCCACGGAAGTTCGG
mus Rps29-R	GAAGCACTGGCGGCACATG
mus Aldh1l2-F	ACTTTCTACGGCTCATCACTGTTG
mus Aldh1l2-R	GGCTTCTTGGCACCTCTAATGTC
mus Gpt2-F	GGTGAAGGCGGTGGAGTACG
mus Gpt2-R	TGGCTCGGATTACCTCAGTGAATG
Mus β-actin-F	GGCTGTATTCCCCTCCATCG
Mus β-actin-R	CCAGTTGGTAACAATGCCATGT

Table S4. ChIP-qPCR primer sequences.

PRIMER TYPE	SEQUENCE 5' → 3'
Slc1a4-F	CCATCCACCCACTCCTTTGT
Slc1a4-R	CTCGGCAGTTCTTCTCCTCAG